A CLOSED FORM ANALYTICAL SOLUTION FOR A SIMPLIFIED WEAR-TYPE RAIL CORRUGATION MODEL

Song, N*, Meehan, P.A.

University of Queensland, Department of Mechanical Engineering, St Lucia, Queensland

Abstract

Wear-type rail corrugation, a longitudinal surface profile irregularity, is predicted as a closed form analytical solution for wear variations about constant nominal wear. This prediction is based on a two-mode model and a wear-type rail corrugation growth analysis of [7]. The wear profile is comprised of a superposition of wear variation for each vibration mode of interest. The solution can be presented either as a first order approximation with reasonably good accuracy, or as a full series expression. The solution is tested and compared with numerical simulations under various parameter conditions. Good agreement between analytical and numerical results has been found. After the wear profile prediction is obtained, the growth rate is derived in the time and frequency domains. The effect of an initial impulse, representing a rail surface irregularity, on the growth rate measurements is investigated and found to be significant. The closed form analytical growth rate results are shown to agree with numerical simulations of the two-mode model and the simplified growth rate expression derived previously.

Nomenclature

C_ξ	Nondimensionalised creep coefficient
$\mathbb{F}$	Fourier transform operator
G_{r_i}	Growth rate parameter for mode i
h_b	Bump height representing rail profile irregularity magnitude
h_i	Modal bump height representing rail profile irregularity magnitude
k_0	Wear coefficient
k_c	Contact stiffness
K_b	System parameter, representing the sensitivity of wear variations to wheel/rail contact deflection variations
K_{c_i}	System parameter, representing the modal sensitivity of wheel/rail relative displacement to input longitudinal profile
Ł	Laplace transform operator
m_i , ω_i , ζ_i	Modal mass, natural frequency, damping
n	Number of modes
N	Wheelset pass number
p_i	Element of the modal matrix
P_0	Nominal contact force
S	Nondimensionalised Laplace transform complex variable
t	Dimensional time
V	Train speed
x	Distance along rail track
y_i , Y_i	Time, Laplace domain modal displacement of vertical wheelset rail dynamics
y_r	Vertical displacement of rail
y_w	Vertical displacement of the wheelset
z_{in} , Z_{in}	Time, Laplace domain rail longitudinal profile irregularity from nominal steady state wear conditions entering the rolling contact region
z_{out} , Z_{out}	Time, Laplace domain rail longitudinal profile irregularity from nominal steady state wear conditions exiting the rolling contact region
α , β_i	System parameter
δ	Delta function
τ	Nondimensional time
ω_d	Nondimensional damped oscillation frequency
Ω	Nondimensional frequency domain variable
Δz_0	Nominal steady state change in profile per wheelset pass
$\Delta\tau$	Nondimensional impulse duration or bump action time

Subscript

i	Modal parameter

Introduction

The evolution of rail corrugation has been studied for several decades. In the last two decades, wear-type corrugation, characterized by both a long (100-400mm) and short pitch (25-80mm) wavelength, has aroused railway industry concerns. Currently the only reliable remedy for this problem is grinding which costs the industry substantially. Other techniques, such as rail hardfacing, have had some reported success in reducing the growth of corrugations but are not reliable cures for all conditions. Therefore much research has been focused on prediction and prevention of rail corrugation recently. Recent research in Germany [1], Sweden [2] and Japan [3] amongst others has resulted in the development of integrated simulation programs incorporating complex finite element models for the dynamics of the track and discrete element models for the rolling contact mechanics. However, as in many practical problems, a fast and exact analytical solution is still required to

confirm these numerical results and provide more insight. The advantage of an analytical solution is that it clearly identifies how the various parameters influence corrugation generation. A number of efforts have been directed towards obtaining analytical solutions to rail corrugation development including Bhaskar et al [4], Muller [5] and Nielsen [6]. Muller [5] and Nielsen [6] have investigated a non-linear contact mechanics filter on wear-type corrugation growth. However the investigation neglected the effect of wheel/rail structural dynamic components on growth. Bhaskar et al and Muller investigated the stability of the interaction between the structural dynamics and contact mechanics. However, both these stability analyses only considered the system behavior over one wheelset passage, neglecting the effect of wear over multiple wheelset passages. Recently, Meehan et al [7] has extended this research providing an analytical prediction of the growth of wear type rail corrugation over multiple wheelset passes. This analytical solution for growth of amplitude of corrugations is based upon a simplified feedback system encapsulating the interactions between the most critical modal dynamics of the vehicle and track, the linearized contact mechanics and the wear process. However, the detailed analytical solution for the complete corrugation wear profile evolution was not explicitly found.

The aim of present work is to extend this analysis of [7] to develop this explicit analytical solution for rail wear profile, initiated by a surface irregularity. In particular, a general mathematical solution for profile variation after a number of wheelset passages, *N,* is first developed based upon a modal analysis of the dynamics [7]. To validate the solution, the results are compared with numerical simulations of a more complex model under various parameter conditions. Subsequently, the growth of wear-type rail corrugation is derived in the time and frequency domains from the analytical solution. In particular, the effect of an initial impulse, representing a rail surface irregularity, on the growth rate measurement is investigated. Finally a comparison of the present analytical results for corrugation amplitude growth with the previously obtained analytical expression in [7] as well as the numerical results is performed.

Analytical Solution for Rail Corrugation Profile Variations

The system diagram shown in Figure 1 describes the wear-type rail corrugation development feedback mechanism. Meehan et al [7] provides a detailed description and derivation of this model. The wheelset track vibrational dynamics, I, may be described by the decoupled equation of motion for each mode, in the real analytical form,

$$\ddot{y}_i + 2\zeta_i\omega_i\dot{y}_i + \omega_i^2 y_i = k_c z_{in}(p_i - 1)/m_i \ . \qquad (1)$$

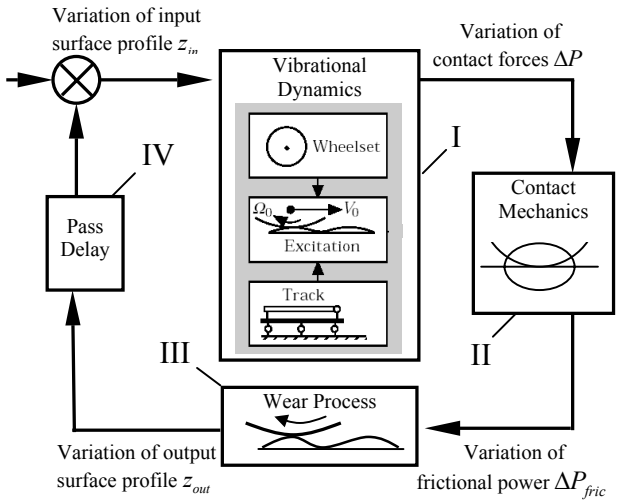

Figure 1. Feedback model for wear-type rail corrugation

The coordinate transform for the modal displacements, y_i, are given by,

$$y_w = \sum_{i=1}^{n} p_i y_i \ , \ y_r = \sum_{i=1}^{n} y_i \ . \qquad (2)$$

The equations governing the contact mechanics, II, and wear process, III, can then be combined and solved for each mode to give,

$$\left(z_{out_i} - z_{in_i}\right)\Big/\Delta z_0 = C_\xi k_c \left(y_i\left(1 - p_i\right) + z_{in_i}\right)\Big/P_0 \ . \qquad (3)$$

Using the Laplace transform denoted as,

$$Ł\ \left\{f\left(\omega_i t\right)\right\} = F(S) \ , \qquad (4)$$

equations (1) and (3) may be solved to obtain,

$$Z_{out_i}/Z_{in_i} = 1 + K_b\left[1 - K_{c_i}\Big/\left(S^2 + 2\zeta_i S + 1\right)\right], \qquad (5)$$

where,

$$K_b = C_\xi k_c \Delta z_0 / P_0 \ , \ K_{c_i} = k_c(1 - p_i)^2 / m_i\omega_i^2 \ . \qquad (6)$$

Equation (5) may be used to determine the profile after N passes. From definition, the profile coming into the contact patch, $Z_{in_i N}$, is the same as profile after the previous pass, $Z_{out_i N-1}$, i.e. $Z_{in_i N} = Z_{out_i N-1}$ representing the pass delay, IV. Using this simplification, the expression for the profile after N passages, $Z_{out_i N}$ may been obtained as,

$$\frac{Z_{out_i N}}{Z_{in_i 1}} = \frac{Z_{out_i 1}}{Z_{in_i 1}}\frac{Z_{out_i 2}}{Z_{in_i 2}}\cdots\frac{Z_{out_i N}}{Z_{in_i N}} = \alpha^N\left(1 - \frac{\beta_i}{S^2 + 2\zeta_i S + 1}\right)^N , \qquad (7)$$

where system parameters α and β_i are defined as,

$$\alpha = 1 + K_b \ , \ \beta_i = K_b K_{c_i}\Big/\left(1 + K_b\right) . \qquad (8)$$

Using a Taylor's series expansion for the *N*th order difference function, equation (7) may be expressed as,

$$\frac{Z_{out_i N}}{Z_{in_i 1}} = \alpha^N \left[1 + \sum_{j=1}^{N} (-1)^j \binom{N}{j} \left(\frac{\beta_i}{S^2 + 2\zeta_i S + 1} \right)^j \right], \quad (9)$$

where the binomial coefficient is defined as ,

$$\binom{N}{j} = \frac{N!}{j!(N-j)!}.$$

In the subsequent analysis, a complete time domain solution to (9) is developed for an initial bump or impulse condition representing a typical irregularity of the rail. In the Laplace domain, the magnitude of the initial profile, $Z_{in_i 1}$, is defined as the area under the impulse. In the time domain, the magnitude of the initial profile, $z_{in_i 1}$, is defined as height of the impulse function.

The inverse Laplace transform of (9) is the time domain rail longitudinal profile after *N* passages in response to an impulse, and may be obtained as,

$$z_{out_i N}(\tau) = \alpha^N \left\{ h_i \delta(\tau - \Delta\tau) + h_b \Delta\tau \sum_{j=1}^{N} \left[(-1)^j \binom{N}{j} \beta_i^j L_N \right] \right\}, (10)$$

where,

$$L_N = \frac{-e^{-\zeta_i \tau}}{4^{N-1} \omega_{d_i}^{2N}} \sum_{r=1}^{N} \binom{2N-r-1}{N-1} \frac{(-2\tau)^{r-1}}{(r-1)!} \frac{d^r}{d\tau^r} \left[\cos(\omega_{d_i} \tau) \right]$$

and $\omega_{d_i} = \sqrt{1-\zeta_i^2}$. The nondimensional time is defined as $\tau = \omega_i \cdot t$. The modal contribution to the impulse response is defined by,

$$h_i = K_{c_i} h_b , \quad (11)$$

where $\sum_{i=1}^{n} h_i = h_b$. The total wear is then obtained as,

$$z_{out N}(\tau) = \sum_{i=1}^{n} z_{out_i N}(\tau) . \quad (12)$$

As an example, equations (10), (11) and (12) may be used to obtained the wear profile after the first pass, as,

$$z_{out_i N}(\tau) = \alpha^N \left[h_i \delta(\tau - \Delta\tau) - h_b \Delta\tau N \beta_i e^{-\zeta_i \tau} \frac{\sin(\omega_{d_i} \tau)}{\omega_{d_i}} \right] (13)$$

This solution also represents the first order approximation for wear over subsequent passes.

By inspection of (10), it is noticed that for *N* passages, the first *N* terms should be included in the solution for perfect accuracy. However, large amounts of computer memory are required for large values of *N*. Therefore, it is useful to determine how many terms are required to achieve sufficient accuracy.

Wear Prediction Comparison

The explicit analytical solution for rail profile wear (10-12) was compared with that obtained via numerical integration. An example of the results is shown in Figure 2. In particular, the wear prediction (10-12) with one (13) and three terms is plotted versus rail track position variable, *x*, assuming constant vehicle velocity *V=xt*. For comparison numerical simulations using the simplified numerical model of (7) with parameters of Table 1 are also plotted for the case with $k_0 = 10^{-6} \left[kg/Nm \right]$.

Table 1. Railway parameters for simulation

Train speed [m/s]	22	Track length [m]	6~33
Wheel mass [kg]	350	Rail density [kg/m]	7700
Wheel radius [m]	0.46	Rail radius [m]	0.3
Wheel load [kN]	66	Coef. of friction	0.4
Young's modulus (Steel) [N/m^2]	2.1×10^{11}	Primary rail Damping	0.01
Poisson's ratio	0.3	Bump length [mm]	0.25~2.5
Shear modulus [Pa]	7.7×10^{10}	Bump height [m]	10^{-6}
Sleeper spacing [m]	0.6	Contact damping	0.0021

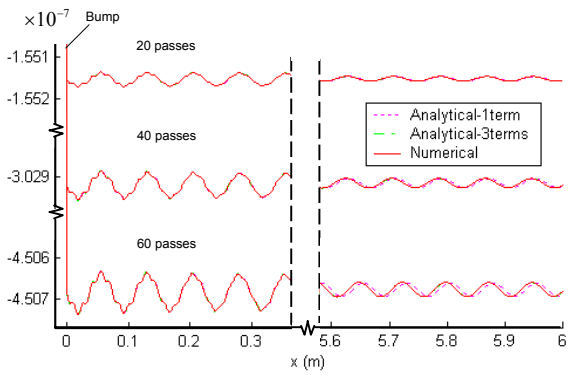

Figure 2. Wear profile time history prediction

Figure 2 shows a very good correlation between the numerical and analytical profile predictions at the initial section of the rail span. It is noted that in this section of the plot all solution traces are overlapping one another. The wavelength of corrugation is determined by the dominant modal frequency of the system and the speed of the vehicle. In this case the lower frequency system mode at 295Hz has a higher growth rate and therefore dominates over the higher frequency mode at 1503Hz. It is noted that the three-term solution consistently overlaps the numerical results, while the one term solution is sufficient if the local wear, in the vicinity to a bump, is of interest. These results indicate that at least three terms should be included in the solution for a fairly accurate result over the full length of track. In general, similar agreement between the analytical and numerical time history results has been obtained for a range of k_0 . It is noted that this agreement deteriorated as the length of the initial bump increased; ie as the initial conditions became less like an impulse.

Growth Rate Prediction

It is of interest to determine and compare the growth rate of the amplitude of wear variations from the full analytical solution (10-12) with those obtained numerically and by use of the simplified expression developed in [7]. The growth rate may be obtained in the time or frequency domain. In the time domain, peak and trough values of wear profile variation, may be used to measure growth in amplitude of wear over successive passages. Alternatively, in the frequency domain, a discrete Fourier transform algorithm (FFT) may be used for the same purpose.

The results obtained by these two means are analyzed and compared with numerical simulations. The reason for an unexpected difference between results is revealed via a frequency domain analysis of the entire wear profile.

Time Domain Growth Rate Measurement

With time domain wear, the growth rate may be obtained by individual measurement of the peaks and troughs of profile after the irregularity (bump) to obtain the profile magnitude ratio $Z_{out_i N}/Z_{in_i N}$ for each mode at a particular rail span position, *x*. This method is found to require a large number of passages to be accurate. The reason for this is numerical in nature. For instance, using the one-term approximation (13) the profile ratio after *N* passes is,

$$Z_{out_i N}/Z_{in_i N} = \alpha\, N/(N-1), \qquad (14)$$

where α is 1.000092 for the parameters of Table 1 and $k_0 = 10^{-6}$. By inspection of (14) it can be seen that a substantial pass number related error arises from the factor $(N-1)/N$. In this case, this error factor takes the values 2, to 3/2, 4/3 over successive passes and decreases slowly toward unity as *N* increases. In fact, simulation revealed that a pass number independent growth rate could be seen only after 10^5 passages when the term $(N-1)/N$ drops below 1.00001. This poses a large calculation burden for computer simulation. Unfortunately artificially increasing the wear rate coefficient, k_0, to scale to a larger number of passages, causes the contact force to vary beyond the linear range, therefore inducing another source of error.

One possible method to overcome this pass number dependent error in growth rate is to multiply the measured profile ratio $Z_{out_i N}/Z_{in_i N}$ by an operating factor $(N-1)/N$ for a one-term approximation. In this case, in accordance with (14) a growth rate of α would be expected to be obtained for the dominant mode. However, using this method there is not a distinct measurable growth rate for each mode. For higher order approximations, the factor $(N-1)/N$ inevitably introduces errors into higher order terms. These higher order terms later are found to have a greater contribution further away from bump. Hence only when choosing the first few peaks at the initial position of the rail span, does a fairly accurate growth rate appear to be obtained using this method. An example of a growth rate plot using this method is shown in Figure 3.

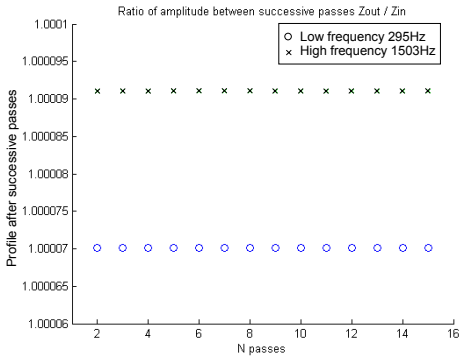

Figure 3. Modal growth of the amplitude of the first peak-trough of profile with 6-term formula

From the graph, the growth rate of low and high frequency mode corrugations is estimated as 0.00007 and 0.00009 respectively. It is of interest to compare these growth rate results to those obtained in [7]. In [7] the dominant frequencies that give extreme values for growth are $\omega_d^{\,2} = 1 + 2\zeta_i$ and $\omega_d^{\,2} = 1 - 2\zeta_i$ and the corresponding maximum growth rate derived is ,

$$G_{r_i} \approx K_b\left(1 + K_{c_i}/4\zeta_i\left(1+\zeta_i\right)\right), \qquad (15)$$

assuming a small k_0, where G_{r_i} is defined as,

$$Z_{out_i}/Z_{in_i} = e^{Gr_i}. \qquad (16)$$

Following the stability analysis as in [7], if the modal frequencies $\omega_{d_i} = \sqrt{1-\zeta_i^{\,2}}$ of the harmonic components of (10) are used instead of the extreme values above, the corresponding growth rate is obtained as,

$$G_{r_i} \approx K_b\left(1 + K_{c_i}/\left(3\zeta_i^{\,2} - 4\right)\right), \text{ for } k_0 << \zeta_i. \qquad (17)$$

The modal growth rates calculated using (17) and parameters in Table 1 are 0.7005×10^{-4} and 0.9109×10^{-4} for $k_0 = 10^{-6}$. These values are almost exactly evident in the numerical results of Figure 3, however are distinctly different from those calculated using (15).

Therefore it is found that by using a time domain method that neglects growth over the entire rail profile, the characteristic frequencies of the wear profile appear to differ from the dominant ones predicted in [7]. To investigate these shortcomings further a growth rate analysis in the frequency domain is performed and analytical and numerical results are compared.

Frequency Domain Growth Rate Measurement

A Fourier analysis was performed in order to identify the dominant frequencies associated with the maximum growth rate, taking into account the entire wear profile. For simplicity, the first order approximation of the full analytical solution (13) is considered. The Fourier transform of (13) may be expressed as,

$$\frac{\mathbb{F}\left[z_{out_i1}(\tau)\right]}{A_2} = A\mathbb{F}\left[\delta\left(\tau-\Delta\tau\right)\right]-\mathbb{F}\left[e^{-\zeta_i\tau}\sin\left(\omega_{d_i}\tau\right)\right] \quad (18)$$

where the following amplitude parameters are defined as

$$A_1 = \alpha^N h_i,\ A_2 = \alpha^N h_b \Delta\tau N\beta_i/\omega_{d_i}, \quad (19)$$

$$A = A_1/A_2 = \left(1+K_b\right)\omega_{d_i}/\Delta\tau NK_b\ . \quad (20)$$

The second term of (18) represents the frequency content of the wear profile not including the initial irregularity. This term alone would provide a spectrum peak at $\omega_{d_i} = \sqrt{1-\zeta_i^2}$, in accordance with the results using the time domain analysis in the previous section. In the following analysis the effect of combining this term with the bump related, δ, term is investigated. In particular, evaluation of the transforms in (18) gives,

$$\mathbb{F}\left[\delta\left(\tau-\Delta\tau\right)\right] = A\left[\cos(\Omega\Delta\tau)-i\sin(\Omega\Delta\tau)\right], \quad (21)$$

$$\mathbb{F}\left[e^{-\zeta_i\tau}\sin\left(\omega_{d_i}\tau\right)\right] = \omega_{d_i}/\left(1-\Omega^2+i2\zeta_i\Omega\right). \quad (22)$$

where Ω is the nondimensionalised frequency variable of the Fourier transform. Since the impulse duration time is much smaller than the natural period of damped oscillation $1/\omega_i$, it is assumed that the cosine function in (21) is approximately 1 and the sine function, 0, for frequencies, Ω, of order less than 2. Therefore, under this approximation, the magnitude artifact of equation (21) may be expressed as,

$$\left|\frac{\mathbb{F}\left[z_{out_i1}(\tau)\right]}{A_2}\right|^2 = A^2+\frac{(1-\zeta_i^2)-2A\sqrt{1-\zeta_i^2}(1-\Omega^2)}{\left(1-\Omega^2\right)^2+4\zeta_i^2\Omega^2}. \quad (23)$$

The particular frequency, Ω, that maximizes the magnitude of $\mathbb{F}[z_{out_i1}(\tau)]$, representing the dominant growth rate, may then be determined. The maximum value depends on the second term on the right hand side of (23). Therefore by taking the derivative of this term with respect to Ω and finding the roots, the extreme values of (23) may be determined. The resulting expression is,

$$4\omega_{d_i}\left(1-\Omega^2\right)-8\zeta_i^2\omega_{d_i}-4A\left(1-\Omega^2\right)^2+16A\zeta_i^2 = 0\ . \quad (24)$$

Solving equation (24) results in,

$$\Omega^2 = 1-\frac{\sqrt{1-\zeta_i^2}}{2A}\pm\sqrt{\frac{1-\zeta_i^2}{4A^2}-\frac{2\zeta_i^2\sqrt{1-\zeta_i^2}}{A^2}+4\zeta_i^2}\ . \quad (25)$$

If $1/A << \zeta_i < 1$, equation (25) may be simplified to,

$$\Omega^2 = 1\pm 2\zeta_i\ , \quad (26)$$

which coincides exactly with the theoretically obtained dominant frequencies in [7]. The positive sign in (26) provides a maximum and negative sign results in a minimum. By inspection of equations (19) and (20), it may be deduced that A generally satisfies the condition above, although for a very large number of passes, N, this may not be true.

To this end, the analysis has shown that the FFT of the entire wear profile including the initial impulse shows local extreme values at frequencies in line with [7], while without the impulse there is only one local peak at the damped natural frequencies, ω_{d_i}.

The results of this analysis is confirmed with FFT calculations of numerical simulation results. It is noted the FFT calculations of the analytical solution (10-12) provided the same results as shown in Figure 4. From these results, it may be inferred that the entire wear profile needs to be included to obtain the exact values of the dominant frequencies of the maximum growth rate. The importance of obtaining correct dominant frequencies on growth rate prediction is investigated subsequently.

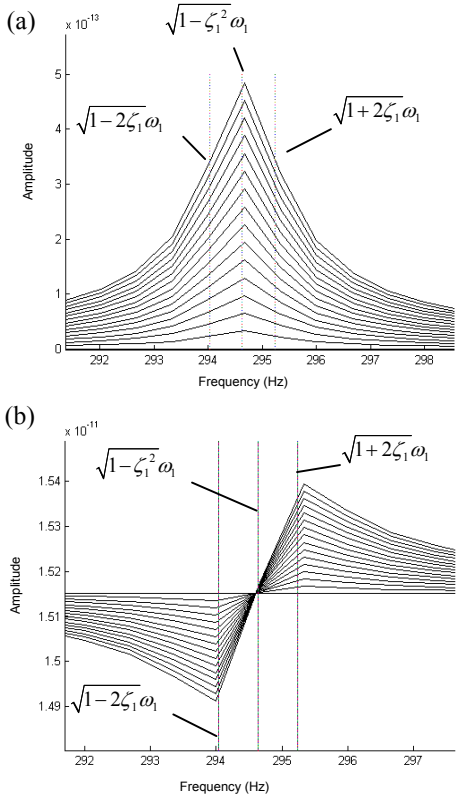

Figure 4. Frequency spectrum of in the region of the low frequency mode of the wear profile; (a) without the initial bump; (b) including the initial bump.

Growth Rate Comparison

The growth rate obtained from the frequency domain method is compared with results via numerical simulation, and the analytical expression (15) (of [7]) in Figure 5 using the parameters of Table 1 and $k_0 = 10^{-7}$ kg/Nm. The wear is expressed as a profile ratio, which is defined as $z_{out_i N} / z_{in_i 1}$ for the lower dominant frequency mode of wear. The full analytical solution (10-12) was used with a range of different accuracies and all converged to the trace marked as 'Full analytical'. Table 2 summarizes the results for growth rate derived using the three methods for both the low and high frequency modes.

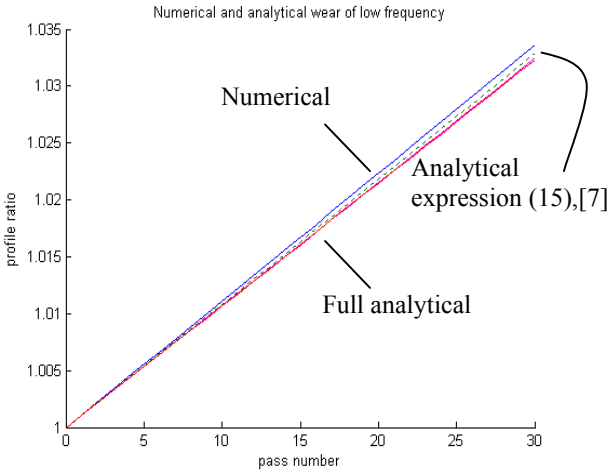

Figure 5. Profile ratio comparison of low frequency

Table 2. Growth rate comparisons

	G_r of low frequency	G_r of high frequency
Numerical	0.01097	0.000203
Analytical (14)	0.01079	0.000188
Full analytical	0.01065	0.000191

The results of figure 5 and Table 2 show that for both lower and higher frequency modes of wear, very good agreement between all methods is obtained. The significance of obtaining the exact dominant frequencies of the wear may be noted. In particular, the growth rates obtained in Table 2 for the lower and higher frequency mode is in the order of 1400 times and 20 times higher, respectively, than that obtained using the time domain method.

In the above analysis it has been shown that the entire wear profile including the initial irregularity needs to be incorporated via an FFT analysis when estimating corrugation growth. Also, the results indicate that the analytical expression (15) of [7] is a sufficiently accurate tool for corrugation growth estimation.

Conclusions

A complete analytical solution of the longitudinal corrugation profile initiated by a surface irregularity, represented as a bump has been developed. The solution predicts the rail wear variation over any number of wheelset passes. Wear profile predictions show good agreement with numerical results. Subsequently, the growth rate of wear corrugation derived from this full analytical solution is obtained using time and frequency domain methods. Good results are found using FFT analysis over the entire wear profile including the initial irregularity. In particular, the effect of an initial impulse on the growth measurement results has been analyzed and found to be crucial. The growth rates obtained via numerical simulation and the complete analytical expression support the simplified analytical expression for growth rate obtained in [7].

A limitation of this closed form solution is that by linearization, it has been assumed that the growth amplitude is small. Therefore, for larger amplitude growth it is expected that the comparisons between numerical and analytical solutions will deteriorate, due to nonlinearities.

Future investigations could focus on the influence of sleepers and nonlinearities of the creep model. Also, it is of interest to investigate more deeply the effects of wheel speed and initial rail irregularity size on growth.

References

[1] K. Hempelmann and K. Knothe, An extended linear model for the prediction of short pitch corrugation, Wear 191 (1996) 161-169

[2] A. Igeland, and H. Ilias, Rail Head Corrugation Growth Predictions Based On Non-Linear High Frequency Vehicle/Track Interaction, Wear 213 (1997) 90-97

[3] A. Matsumoto, Y. Sato, et al. Study on the Formation Mechanism of Rail Corrugation on Curved Track. Vehicle System Dynamics 25 (1996) 450-465

[4] A. Bhaskar, K.L. Johnson, G. D. Wood, and J. Woodhouse, Wheel-rail dynamics with closely conformal contact. Part 1. Dynamics Modeling and Stability Analysis, Proc. Instn. Mech. Eng. 211 (F) (1997)11-26

[5] S. Muller, A linear wheel-rail model to investigate stability and corrugation on straight track, Wear 249 (2001) 1117-1127

[6] J. B. Nielsen, Evolution of rail corrugation predicted with a non-linear wear model, Journal of Sound and Vibration 227 (1999) 915-933

[7] P.A. Meehan,W.J.T. Daniel and T. Campey, Wear-type rail corrugation prediction and prevention, Proceedings of the 6th International Conference on Contact Mechanics and Wear of Rail/Wheel Systems(CM2003) in Gothenburg, Sweden, June 10-13, (2003) 445-454